A forward model of three-dimensional fracture orientation and characteristics

K. Tuncay, A. Park, and P. Ortoleva

Laboratory for Computational Geodynamics, Department of Chemistry, Indiana University, Bloomington

Abstract. A new forward modeling approach to simulate the extension/closure and orientation statistics of evolving fracture networks is presented. The model is fully dynamical and couples fracturing to other processes. Thus, fracturing affects hydrology and, in turn, its development is affected by fluid pressure. In this way, highly pressured fluids can enhance their own migration while low-pressured ones may become trapped. Fracturing affects the stress tensor through rock volumetric changes and stress affects fracture dynamics. Thus, to predict fracture dynamics, we coevolve a set of fracture variables simultaneously with mass, momentum, and energy conservation equations for the solid and multiple fluid phases. In our computational approach, a representative set of putative fractures of a range of orientations is introduced. The time-dependent properties of each realized fracture is calculated by using the stress component normal to its fracture plane, pressure, and rock properties. The volumetric strain caused by fracturing allows for a self-limiting feedback that we account for using a nonlinear incremental stress rheology. The anisotropic fracture permeability is obtained using the predicted fracture network statistics. Thus, the coupling between rock deformation, notably fracturing, and hydrology is accounted for as is that between fracturing and stress. The statistical aspect of fracture network dynamics is described by assuming a probability distribution characterizing variations in rock strength within a nominally uniform lithology. The dependence of fracture density and length on the rate of fluid pressure or stress variation is thereby captured. Embedding the model in a three-dimensional basin finite element simulator, we illustrate the dynamical nature of the location and character of fracture zones in a sedimentary basin.

1. Introduction

Fractures play an important role in many geologic processes. They provide a mechanism of deformation and a pathway for fluid flow. The timing of fracture initiation and the scenario of their evolution over the history of a zone may significantly affect the rate and direction of fluid migration. Fractures provide a mechanism of time-dependent (that is, irreversible) and directional deformation. To address these problems, we develop a kinetic model of the evolution of the three-dimensional character of fracture networks.

Because of its importance to both petroleum and geological sciences, fracturing has been studied by many researchers (see *Pollard and Aydin* [1988] and *Lorenz et al.* [1991] for reviews). Fractures in areas subjected to bending are usually explained by associated extensional stresses [*Friedman*, 1975]. The existence of fractures in near-horizontal layers has been attributed to unloading [*Currie and Nwachukwu*, 1974; *Engelder*, 1987], high fluid pressure [*Pollard and Aydin*, 1988; *Ortoleva*, 1998], and anisotropic stress influenced by nearby geologic structures [*Segall and Pollard*, 1983; *Currie and Nwachukwu*, 1974]. We believe that fracturing in near-horizontal or folded areas is due to a combination of the effects listed above. If the local fracture kinetics is well described by fracture growth/healing laws, a multiprocess deformation model coupled to fluid flow and fracturing can be used to quantify the relative importance of these effects.

It is well documented that fracturing strongly depends on lithology [*Segall and Pollard*, 1983; *Lorenz et al.*, 1991; *Fischer et al.*, 1995; *Gross*, 1993; *Wu and Pollard*, 1995; *Hancock et al.*, 1984; *Kulander et al.*, 1979]. Although fracturing can occur in almost any type of rock, fractures are more common in brittle rocks [*Mallory*, 1977]. Furthermore, fractures in a brittle lithology commonly discontinue at the interface of more ductile lithologies [*Engelder and Geiser*, 1980]. Another observation is that fracture spacing is strongly dependent on bed thickness and lithology [*Fisher et al.*, 1995; *Wu and Pollard*, 1995; *Gross*, 1993; *Nickelsen and Hough*, 1967; *Harris et al.*, 1960] However, a simple correlation between fracturing and bed thickness does not seem feasible because of the many factors operating such as fluid pressure, state of stress, neighboring lithology properties, and tectonics.

Dynamic fracture models are needed in a petroleum engineering context. As fluid pressure is drawn down, fractures can close and destroy reservoir quality. Thus a reservoir model must account for the coupling of the fluid pressure, fracture network characteristics, and the stress field, all of which coevolve in an inextricably coupled manner.

Petroleum expulsion from source rocks, migration, and leakage from reservoirs are key aspects of the dynamic petroleum/fracture system. Many petroleum reservoirs worldwide would not be producible if it were not for the presence of fractures. Fractures provide efficient conduits for mineralizing fluids either from within a sedimentary basin or of deep crustal origin. To understand these phenomena, we have developed a model that predicts the evolution of the fracture network that can be coupled to the fluid pressure, stress, and rock rheologic properties. Even if one only is interested in present-day fracture network location and characteristics, it is

necessary to unravel the past as the rate of change of the aforementioned parameters significantly affects the fracture network. In short, present-day fracture length, orientation, and intensity statistics are a reflection of past history.

Present-day flexure is often a poor indicator of fracturing. If the rate of flexure development was very slow, then there would be no fracturing. Also, flexure early in a sedimentary rock's evolution (i.e., when it is poorly lithified) or if sediment has inherent ductile behavior (as for organic-rich shales, rock salt, or anhydrites) can occur without fracturing. Thus prediction of present-day fracturing requires a model that allows for the continuous processes (notably ductile behavior or pressure solution) to compete with discontinuous deformation (faulting and fracturing) to arrive at the overall deformation.

To account for this competition between continuous and discontinuous processes, we integrate a full suite of deformation processes within an incremental stress format. The formal statement of the incremental stress rheology [Ortoleva, 1994a, 1998; Tuncay et al., Sedimentary basin deformation: An incremental stress approach, submitted to Tectonophysics, 2000 (hereinafter referred to as Tuncay et. al., submitted manuscript, 2000)] may be written as

$$\underline{\dot{\varepsilon}} = \underline{\dot{\varepsilon}}^{(pe)} + \underline{\dot{\varepsilon}}^{(vp)} + \underline{\dot{\varepsilon}}^{(ps)} + \underline{\dot{\varepsilon}}^{(go)} + \underline{\dot{\varepsilon}}^{(fr)}. \qquad (1)$$

Here $\underline{\dot{\varepsilon}}$ is the rate of strain tensor (i.e., the derivation of the rock deformation velocity with respect to space)

$$\underline{\dot{\varepsilon}}_{ij} = \frac{1}{2}\left(\frac{\partial u_i}{\partial x_j} + \frac{\partial u_j}{\partial x_i} \right), \qquad (2)$$

where u is the rock deformation velocity with components u_i ($i=1,2,3$), and x_i ($i=1,2,3$) are the three directions of Cartesian space. The contributions to $\underline{\dot{\varepsilon}}$ in (1) are from poroelasticity (pe), viscoplastic mechanical processes (vp), pressure solution (ps), gouge (go), and fracturing (fr). Each of these individual terms depends on rock texture, macroscopic stress $\underline{\sigma}$, fluid pressure, and composition and temperature. Solving equations (1) and (2) and an equation for force balance yields the deformation velocity $\underline{\dot{\varepsilon}}$ and the macroscopic stress $\underline{\sigma}$. In our approach we simultaneously solve these equations with those of multiphase conservation of mass, textural evolution, and heat transfer so as to coevolve most key factors in crustal evolution [see Ortoleva, 1994a, 1998; Ortoleva et al., 1997; Tuncay et al., submitted manuscript, 2000].

Fracturing may introduce anisotropy to the evolving system. Fractures orient flows along their surface and also introduce directions of weakness in a deforming rock. Thus fractures may guide the direction of high-pressure fluids which thereby changes the location of subsequent fracturing. Fracture-induced changes in rheological parameters may affect the overall stress tensor which, in turn, affects the orientation of subsequent fracturing. Thus the pe, vp, and fr terms in (1) can depend on fracture network characteristics.

To account for the above effects, the present fracture model allows for the following: (1) fracture orientation reflecting the stress tensor; (2) the addition of new fractures to the evolving network as the stress tensor changes due to tectonics or to fracture or diagenetic changes in rheology; (3) how the fracture network characteristics affect the tensorial fluid transport (e.g., permeability) and rock rheologic parameters; (4) the construction of rose diagrams and other parameters which can be compared with observation; and (5) the mineralogy, texture, and statistical variations of properties (notably weak spots) that can affect fracturing and which change over the geological timescale.

Development of a fracture network involves the coupling of stresses, fluid pressure and composition, rock rheology, and the nucleation, growth or dissolution of mineral grains. The premise of the present model of hydrofracturing is that these features are small in scale compared to the spatial scale of the fracture network. All fracture and other textural variables are assumed to vary continuously in space across a system. Thus it is assumed that fracture length is smaller than bed thickness or the radius of curvature of a flexure.

In most crustal evolution models, it is assumed that rocks fracture when the fluid pressure exceeds a specified fraction of lithostatic stress [Maubeuge and Lerche, 1993, 1994; Roberts and Nunn, 1995; Wang and Xie, 1998]. This assumption essentially eliminates the dependence of fracturing on lithologic properties although it is well known that fracturing strongly depends on texture [Lorenz et al., 1991; Segall and Pollard, 1983; Mallory, 1977; Fisher et al., 1995; Wu and Pollard, 1995; Gross, 1993; Nickelsen and Hough, 1967; Harris et al., 1960]. Such a simplification also fails in predicting nonvertical fractures due to flexure.

In most of the existing basin evolution simulators, fracture permeability is assumed to be isotropic [Maubeuge and Lerche, 1993, 1994; Roberts and Nunn, 1995; Wang and Xie, 1998; Ungerer et al., 1990; Schneider et al., 1996; Luo and Vasseur, 1996]. This is apparently due to the lack of information in their models about the tensorial nature of the stress tensor and the resulting, evolving fracture network. Another effect that is always disregarded is the interaction between net deformation, stress, and fracturing. It is true that rocks fracture due to the difference between the fluid pressure and the least compressive stress. However, as fractures open, the overall rock volume increases and fluid pressure in the fractures compresses the rock, increasing the compressive stress normal to the fracture plane. Our model captures this self-limiting process by solving the stress, deformation, fracturing, and fluid flow problems simultaneously.

There is a vast amount of work on approximations for the permeability of fracture networks (e.g., Koudina et al., 1998; Oda, 1986; Long and Billaux, 1987; Berkowitz, 1995; Odling, 1992). However, in these studies, a fracture network is generated either by an independent (decoupled) statistical geometrical model or based on data. Here we address the evolution of a three-dimensional complex fracture network based on fracture growth and initiation laws proposed earlier [Segall, 1984; Atkinson, 1984; Dutton, 1974; Wang et al., 1983; Sonnenthal and Ortoleva, 1994; Brantley et al., 1990].

The approach presented here is based on a dynamical model of fracture growth that is fully coupled to other crustal processes, deformation, and heat transfer. Thus the oscillatory and other self-organization and nonlinear phenomena of crustal evolution can be captured [Ortoleva et al., 1987a, b; Ortoleva, 1994a, b; Dewers and Ortoleva, 1994; Maxwell, 1997; F. Renard and P. Ortoleva, manuscript in preparation, 2000]. The most notable of these is the cycle of fracturing → fluid flow → fluid pressure release → fracture healing [Ghaith et al., 1990; Chen et al., 1994; Dewers and Ortoleva, 1994; Ortoleva, 1998].

In the following section, we describe models for subcritical crack growth similar to that implemented by Dewers and Ortoleva [1992], Sonnenthal and Ortoleva [1994], and Maxwell [1997]. Modifications were made to the fracture length growth law that allows for fracture healing. In these models, each representative volume of rock is given a statistical distribution of fracture nuclei and associated tensile strength. This is a way to approximate the effect of rock heterogeneity and fracture interaction, and to predict the density of fractures and their dependence on the histories of stress, fluid pressure, and rock properties. A formalism is developed to ac-

count for the orientation of single or multiple fracture sets. The model is thereby able to describe conditions for developing a few large fractures or a swarm of smaller ones, depending on the rate of change of fluid pressure and stress. The change in the rock volume and anisotropic fracture permeability tensor are obtained. Numerical examples illustrating some aspects of our dynamic fracture statistics model for basin evolution are presented.

2. Single Fracture Dynamics

In this section, a model of the dynamics of an isolated fracture is considered. In the next two sections, this model is used to develop a fracture network statistical dynamics law.

An isolated fracture is found to grow if the crack extension force [Segall, 1984] or the fracture propagation energy [Sonnenthal and Ortoleva, 1994] exceeds critical values. Fractures for which the crack extension force does not exceed the critical value are assumed to heal [Segall, 1984]. The rate F of the change of radius r of an assumed circular planar fracture is taken to have the form [Segall, 1984; Atkinson, 1984; Dutton, 1974]

$$F = v_f[1 - \exp(-U/RT].$$ (3)

The limiting propagation velocity v_f depends on the mechanism of growth. For fractures of interest here, the growth and healing rate limiting kinetic mechanism may be surface, grain-boundary, thin-film diffusion or mineral reaction [Atkinson, 1984; Dutton, 1974; Swanson, 1984; Smith and Evans, 1984]. If fracturing is "reversible" (that is, fracturing and healing take place by the same mechanism), v_f is the same regardless of the sign of F (and hence of U). However, this is often not the case and hence v_f can change with the sign (and likely the magnitude) of U. The factor U in (3) is given by Segall [1984] and Atkinson [1984],

$$U = \frac{V}{a}\left[\frac{\pi(1-v^2)}{E}r\sigma_{ne}^2 - Q\right].$$ (4)

Here

V the molar volume of the solid containing the (nascent) fracture averaged over the volume fractions of all the minerals;

a fracture aperture;

v, E Poisson's ratio and Young's modulus, respectively, for the multimineralic, porous medium;

σ_{ne} component of effective stress (positive for extension) normal to the plane of fracture far from the fracture $(\sigma_{ne} = \sigma_n + p)$;

σ_n component of total stress (positive for extension) normal to the plane of fracture far from the fracture;

Q threshold value of crack extension force.

The first factor in (4) is the fracture propagation energy, and Q is its threshold value required for propagation. Note that when the fracture propagation energy exceeds Q, $U > 0$ and fractures grow $(F > 0)$.

Even if the tectonic environment implies a compressive stress regime, elevated fluid pressure may induce tensile effective stresses sufficient to initiate fracture growth at textural flaws [Pollard and Aydin, 1988]. The threshold fluid pressure p^* is found by setting U to zero in (4),

$$p^* = -\sigma_n + \left[\frac{QE}{\pi(1-v^2)r}\right]^{1/2}.$$ (5)

The second term in (5) can be thought of as the tensile strength of the rock; it decreases with increasing fracture length.

The limiting propagation velocity v_f is taken to have the following temperature and aperture dependence [Wang et al., 1983]:

$$v_f = \frac{v'}{a^m T}\exp\left[-\frac{E_f}{RT}\right],$$ (6)

where v', m, and E_f (an activation energy) are dependent on the rate-determining mechanism for fracturing. Data from Brantley et al., [1990], assuming surface diffusion to be the rate-controlling mechanism, suggests $v' = 10^{-12}cm^6 \,°K/erg·s$, $E_f = 8.0 \times 10^{11}$ erg/mol, and $m = 2$; Q is taken to be 10^4 erg/cm^2, as suggested by Segall [1984] and Atkinson [1984]. It is not clear that these values apply directly to natural hydrofractures in multimineralic, porous rocks. However, we expect that the actual timescale of fluid release is controlled by rates of fluid pressure dissipation and overall tectonics, and other deformation processes. The kinetics of fracture generation in nature (and that given by the preceding mechanism) is sufficiently fast that it is likely not a rate-determining factor in fluid expulsion and deformation. Thus when fractures are actively growing or healing, the system rapidly evolves to a "steady state" wherein U remains small so that σ_n, p, r and a coevolve to keep U small as implied by a large value of v'.

The following is adapted for the fracture aperture a:

$$a = r\sigma_{ne}/E, \; \sigma_{ne} > 0.$$ (7)

When fractures form, σ_{ne} is positive. Also, a increases with fracture radius r as one might expect [Sleep, 1988]. When $\sigma_{ne} < 0$, it may be assumed for simplicity that $a = 0$. However, in a more realistic model, the dynamics of a in a $\sigma_{ne} < 0$ environment can be slow due to slow healing processes (notably associated with the chemically mediated rejoining of the two faces of the fracture disconnected during growth).

Examination of the form of (3) and (4) shows that the effective tensile stress necessary to propagate fractures decreases as the inverse square root of fracture length. This suggests that fractures can grow without bound under constant stress conditions. However, there is a number of limitations on the propagation of fractures. In particular, increases in a and r (1) cause rock dilatation and increase compressive stress and (2) open fluid flow pathways that tend to decrease fluid pressure. Also, as hydrofractures grow, they increase overall pore volume (that is, matrix plus fracture contributions). This tends to decrease fluid pressure [Rice and Rudnicki, 1979; Etheridge et al., 1983] so that fractures may grow only long enough to create sufficient porosity that the condition for hydrofracture growth $(p > p^*)$ is no longer satisfied. Enhanced permeability created by fractures can limit fracture growth by dissipation of fluid pressure [Domenico and Palciauskas, 1988]. Finally, mechanical interaction between propagating fracture tips can limit fracture propagation, such that as a fracture network develops, average fracture spacing is related to average fracture length [Pollard and Aydin, 1988].

A difficulty with the above formulation is that it does not directly describe healing and leaves some ambiguities as to the meaning of the equations as r and $a \rightarrow 0$. To surmount this, consider the reformulation as follows [Ortoleva, 1994a]. Introduce nucleation values r_n and a_n of r and a and modified quantities r^*, a^*, and U^* such that

$$a^* = a_n + \frac{r}{E}\sigma_{ne}\theta(\sigma_{ne}),$$ (8)

$$r^* = (r^2 + r_n^2)^{1/2},$$ (9)

$$U^* = \frac{\pi(1-v^2)V}{Ea^*}\left[r^* \mid \sigma_{ne} \mid \sigma_{ne} - Y\right], \tag{10}$$

where $Y = EQ/\pi(1-v^2)$ and $\theta(x) = 1$, $x > 0$; 0, $x \leq 0$. Note that when $r \gg r_n$, $a \gg a_n$ and $\sigma_{ne} > (Y/r^*)^{1/2}$, the laws (4) and (10) agree with $U, a, r \rightarrow U^*, a^*, r^*$. However, when $\sigma_{ne} < (Y/r^*)^{1/2}$, $F < 0$ and fractures heal (shorten) in the modified laws only. These laws are also well defined as r and a vanish. The quantities r_n and a_n are reasonably taken to be of the order of magnitude of the grain size [Atkinson, 1984]. The present formulation predicts fracture healing when σ_{ne} is large and negative while the original formulation predicts fracture growth.

3. Statistical Fracture Network Dynamics

Heterogeneity of tensile strength and other properties will bring a statistical aspect to the creation of a fracture network. Using the formulation of Ortoleva [1994a], we account for this in our model by considering a statistical distribution of material properties and associated fractures. By using this statistical treatment, a slow increase in fluid pressure will produce a few large fractures (initiated at the weakest points), whereas a rapid increase in pressure leads to a high density of small fractures.

Consider a set of fracture classes labeled $i = 1, 2, \cdots, N_f$. Then let $a^{(i)}$ = aperture of an i-type fracture; $r^{(i)}$ = length of an i-type fracture; and $\eta^{(i)}$ = number of i-type fractures per rock volume. These variables evolve via

$$\frac{Dr^{(i)}}{Dt} = F^{(i)}, \tag{11}$$

$$\frac{\partial \eta^{(i)}}{\partial t} = -\nabla \cdot (\eta^{(i)} \underline{u}), \tag{12}$$

where $F^{(i)}$ is the rate of growth of i-type fractures. The $F^{(i)}$ depend on the tensile strength $\tau^{(i)}$, that is, $[QE/(\pi(1-v^2)r)]^{1/2}$ for an i-type fracture.

The statistics can be introduced by making an assumption on the distributions of the $\tau^{(i)}$ and $\eta^{(i)}$. First define the following set of quantities

$$\eta = \sum_{i=1}^{N_{fr}} \eta^{(i)}, \tag{13}$$

$$\hat{\eta}^{(i)} = \eta^{(i)}/\eta. \tag{14}$$

If we assume that the identity of fractures does not change (that is, they may not have been manifest but they are latently always there and do not switch class), then the $\hat{\eta}^{(i)}$ associated with a given rock material point do not change. Thus by definition of the material time derivative D/Dt, $D\hat{\eta}^{(i)}/Dt = 0$.

Summing (12) over all i yields

$$\frac{\partial \eta}{\partial t} = -\nabla \cdot (\underline{u}\eta). \tag{15}$$

Making the simplifying assumption that $\hat{\eta}^{(i)}$ does not change with diagenesis or other processes, one obtains

$$\hat{\eta}^{(i)} = \text{its value at deposition.} \tag{16}$$

Thus the $\hat{\eta}^{(i)}$ are a set of fixed parameters determined at deposition. In the simulations presented below, we assume

$$\hat{\eta}^{(i)} = b \exp\left[-(i-i^*)^2/4\Delta^2\right], \tag{17}$$

for "typical" class i^* and Gaussian width D. The normalization factor b is given by

$$b^{-1} = \sum_{i=1}^{N_f} \exp\left\{-(i-i^*)^2/4\Delta^2\right\}. \tag{18}$$

In our analysis i^* and D are taken to be $N_f/2$ and 1, respectively. This choice of D gives a narrow distribution which corresponds to a fairly uniform medium. The case of a broad distribution of tensile strength could be considered in our model by taking a larger value of D. It would be valuable to have quantitative rock mechanics experiments on this issue. The $\hat{\eta}^{(i)}$ represent the statistical distribution of the tensile strength for an i-type fracture. Thus a Gaussian distribution, chosen here for simplicity, represents the distribution of fracture nuclei in classes characterizing their rock strength (for example, rock strength is proportional to i and i^* corresponds to typical rock strength). In the computations carried out here we neglect the creation or destruction of fracture nuclei and the variation of their associated tensile strengths arising from diagenesis.

4. Fracture Orientation

Prediction of fracture orientation is a key component of fracture modeling. Orientation affects the flow direction and also results in anisotropy in inelastic rock properties. A predictive reaction, transport, and mechanical (RTM) model should be able to simulate the history of fracture orientation, fracture density, connectivity, and directional preferences, and the effect of these factors on the evolution of stresses.
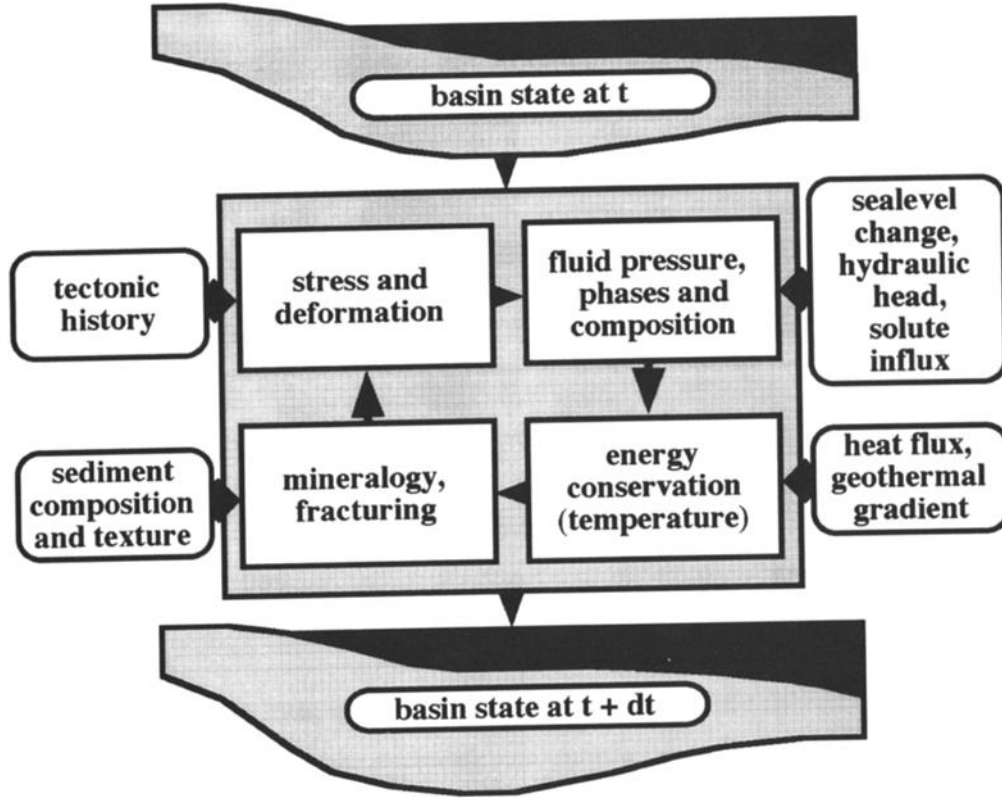
Predicting the orientation of an isolated fracture requires the calculation of the magnitude and direction of least compressive stress. The problem becomes more complex when fractures interact and form a fracture network. To describe these complex phenomena, we have developed the following fracture orientation algorithm. Let i indicate the fracture statistical class (as in the previous section) and ω denote the orientation, that is, one of an assumed discrete set of N_o considered orientations. Thus $N_o N_f$ is the total number of fracture classes allowed. Let $\underline{n}^{(i\omega)}$ be the normal to the i, ω-type fracture. For example, with vertical fractures one has

$$n_x^{(i\omega)} = \cos\left(\frac{\pi}{N_o}(\omega - 1)\right)$$

$$n_y^{(i\omega)} = \sin\left(\frac{\pi}{N_o}(\omega - 1)\right) \tag{19}$$

$$n_z^{(i\omega)} = 0.$$

where $\omega = 1, \cdots, N_o$. The number of fracture orientations N_o is chosen to obtain the desired detail and accuracy. In three dimensions one can write, letting ω denote the pair of indices k, l,

$$n_x^{(i\omega)} = \frac{1}{\zeta}\sin(\phi_k)\cos(\theta_l),$$

$$n_y^{(i\omega)} = \frac{1}{\zeta}\sin(\phi_k)\sin(\theta_l),$$

$$n_z^{(i\omega)} = \frac{1}{\zeta}\cos(\phi_k),$$

$$\phi_k = \frac{\pi}{2m_1}(k-1), \tag{20}$$

$$\theta_l = \frac{\pi}{m_2}(i-1),$$

$$\zeta^2 = (\sin(\phi_k)\cos(\theta_l))^2 + (\sin(\phi_k)\sin(\theta_l))^2 + (\cos(\phi_k))^2,$$

Figure 1. Flowchart showing how the interplay of geologic data and physicochemical (i.e., reaction-transport-mechanical) process modules evolve the basin over a computational time interval δt.

where $1 = 1, \cdots, m_2$ and $k = 1, m_1$. This yields $N_o = m_2/2 + (m_1 - 1)m_2 + 1$ independent orientations (for even m_2). The stress component normal to the fracture plane $\sigma_n^{(i\omega)}$ is calculated from

$$\sigma_n^{(i\omega)} = (\underline{n}^{(i\omega)})^T \underline{\underline{\sigma}} \, \underline{n}^{(i\omega)}, \tag{21}$$

where superscript T indicates a row vector while $\underline{n}^{(i\omega)}$ is represented as a column vector (and $\underline{\underline{\sigma}}$ is a 3×3 matrix). The effective normal stress $\sigma_{ne} = \sigma_n^{(i\omega)} + p$ can be used to obtain the fracture properties such as length and aperture as in Section 2. This approach results in vertical fractures in all horizontal directions in one-dimensional problems as expected physically. For more general cases, it can be used to predict the fracture rose diagrams that are commonly used to characterize observed fracture networks. Finally, the three-dimensional implementation of the approach in deforming systems requires an accounting of fracture rotation as rocks experience flexure or otherwise rotate locally.

5. Rate of Strain, Porosity, and Permeability

In this section, we develop laws of rock deformation and fluid flow that follow from our statistical fracture dynamics model. A phenomenological law for $\underline{\underline{\dot{\varepsilon}}}^{(fr)}$, the contribution to the total rate of strain in an incremental stress rheology [see *Ortoleva*, 1994a, 1998; *Tuncay et al.*, submitted manuscript, 2000] is obtained from geometric considerations. We develop the formula by first considering the dilatation and then conjecturing a tensorial expression for a fracture network.

Let $\Delta^{(i\omega)}$ be the volume density for an i, ω-type fracture:

$$\Delta^{(i\omega)} = \eta^{(i\omega)} \pi (r^{(i\omega)})^2 a^{(i\omega)}. \tag{22}$$

To compute the dilatation, we focus on a fixed volume V_m of solids and follow its change in a time δt. The volume of the unfractured rock V_{unfr} is related to V_m and the porosity ϕ_m of the unfractured rock via $V_{unfr} = V_m + \phi_m V_{unfr}$. Hence $V_{unfr} = V_m/(1 - \phi_m)$. The total volume V of the sample of rock containing V_m is then

$$V = (1 - \phi_m)^{-1} V_m + \sum_{i,\omega} V \Delta^{(i\omega)}, \tag{23}$$

where it has been noted that $V \eta^{(i\omega)}$ is the number of i, ω-type fractures in V. With this the volume of rock $V(t)$ at time t for fixed volume of solids V_m (considered incompressible and not to expand thermally) is given by

$$V(t) = V_m (1 - \phi_m)^{-1} \left[1 - \sum_{i,\omega} \Delta^{(i\omega)} \right]^{-1}. \tag{24}$$
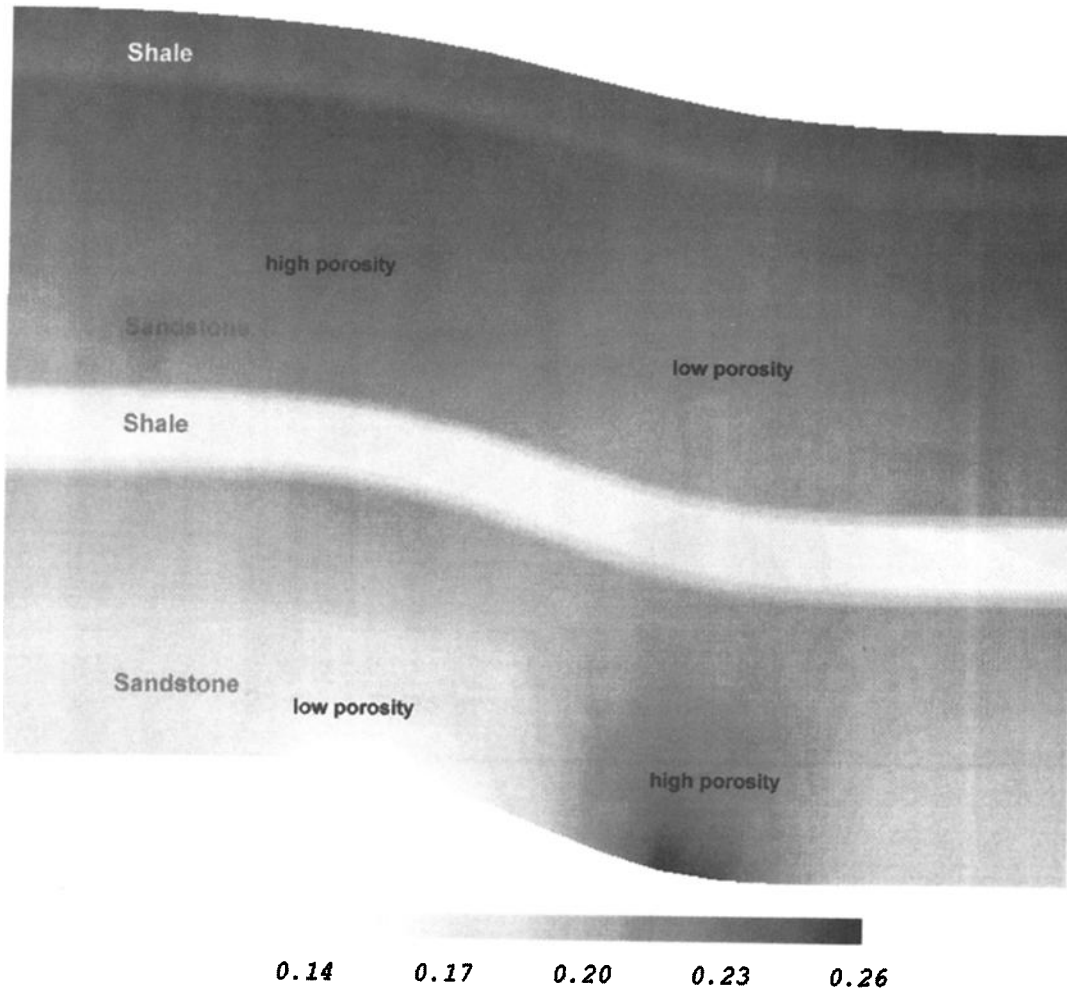
Noting that

$$tr \underline{\underline{\dot{\varepsilon}}}^{(fr)} = \lim_{\delta t \to 0} \frac{V(t + \delta t) - V(t)}{V(t) \, \delta t}, \tag{25}$$

one obtains

$$tr \underline{\underline{\dot{\varepsilon}}}^{(fr)} = \left[1 - \sum_{i,\omega} \Delta^{(i\omega)} \right]^{-1} \sum_{i',\omega'} \frac{D\Delta^{(i'\omega')}}{Dt}, \tag{26}$$

where D/Dt is the material derivative, that is, the derivative in the reference frame fixed to the solids.

The tensor character of the deformation is related to the directionality associated with each fracture type through the normal $\underline{n}^{(i\omega)}$ to the plane for i, ω-type fractures. Consider the expression

Figure 2. Predicted porosity distribution after 5 million years into the simulation showing alternating sandstones and shales two shale layers, the lowest layer being a sandstone layer.

$$\dot{\varepsilon}_{kl}^{(fr)} = \left[1 - \sum_{i,\omega} \Delta^{(i\omega)}\right]^{-1} \sum_{i',\omega'} \frac{D}{Dt}\left(\Delta^{(i'\,\omega')} n_k^{(i'\,\omega')} n_l^{(i'\,\omega')}\right). \qquad (27)$$

Here D/Dt again represents a material time derivative; however, here it also must account for the rotation of the fracture normals as they change direction with flexure, shearing or other deformation. Note that taking the trace of this expression agrees with the earlier result for the dilatation. Finally, this expression agrees with simple cases wherein all fractures are parallel.

It should be noted that the above expressions are strictly valid when the aperture is small relative to fracture length. When a increases at fixed r then one expects some rock shortening in the directions parallel to the fracture plane. As the fractures of greatest interest in geology have small aspect ratio $(a/r \ll 1)$, this is not a limitation of our model. Perhaps a greater limitation is the assumption that fractures are strictly planar and the growth of one fracture does not interfere through tip-tip attractions or intersection. Such complexities and their influence on $\dot{\underline{\varepsilon}}^{(fr)}$ will be considered in subsequent studies.

The total porosity ϕ is computed in a dynamical theory via a conservation of mass consideration. If ρ_s is the mass density of the solids then conservation of mass implies

$$\frac{\partial(1-\phi)\rho_s}{\partial t} = -\nabla \cdot \left[(1-\phi)\rho_s \underline{u}\right]. \qquad (28)$$

When ρ_s is constant, this can be written in the form

$$\frac{D}{Dt}[\ln(1-\phi)] = -\nabla \cdot \underline{u} = -tr\underline{\dot{\varepsilon}}. \qquad (29)$$

Thus if the total rate of strain for all processes is known one can compute ϕ. The porosity is related to the porosity ϕ_x due to the porosity of unfractured matrix and ϕ_f of the fractures. The arguments leading to (23) and (24) indicate that the volume occupied by the pores in the unfractured rock, $\phi_m V_{unfr}$, is given by $\phi_m V_m/(1 - \phi_m)$. Dividing by V as in (24) yields the net porosity from the pores in the matrix, ϕ_x, that is,
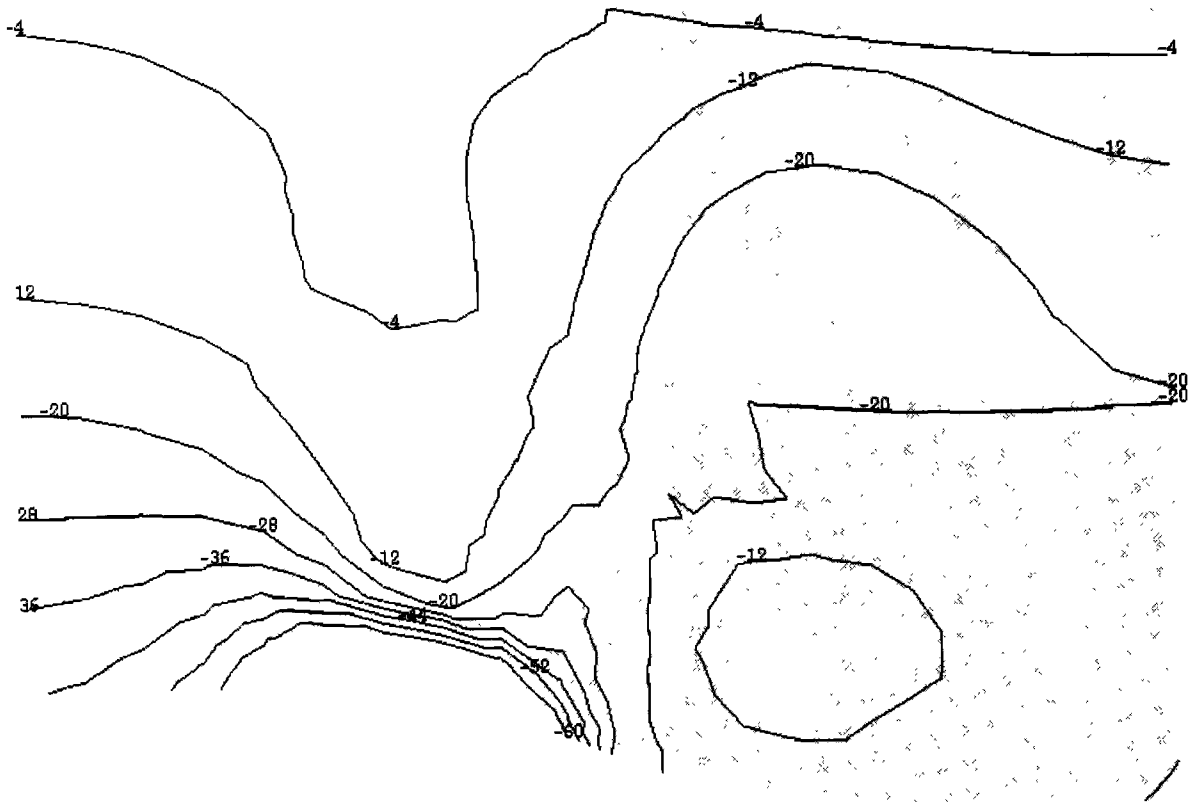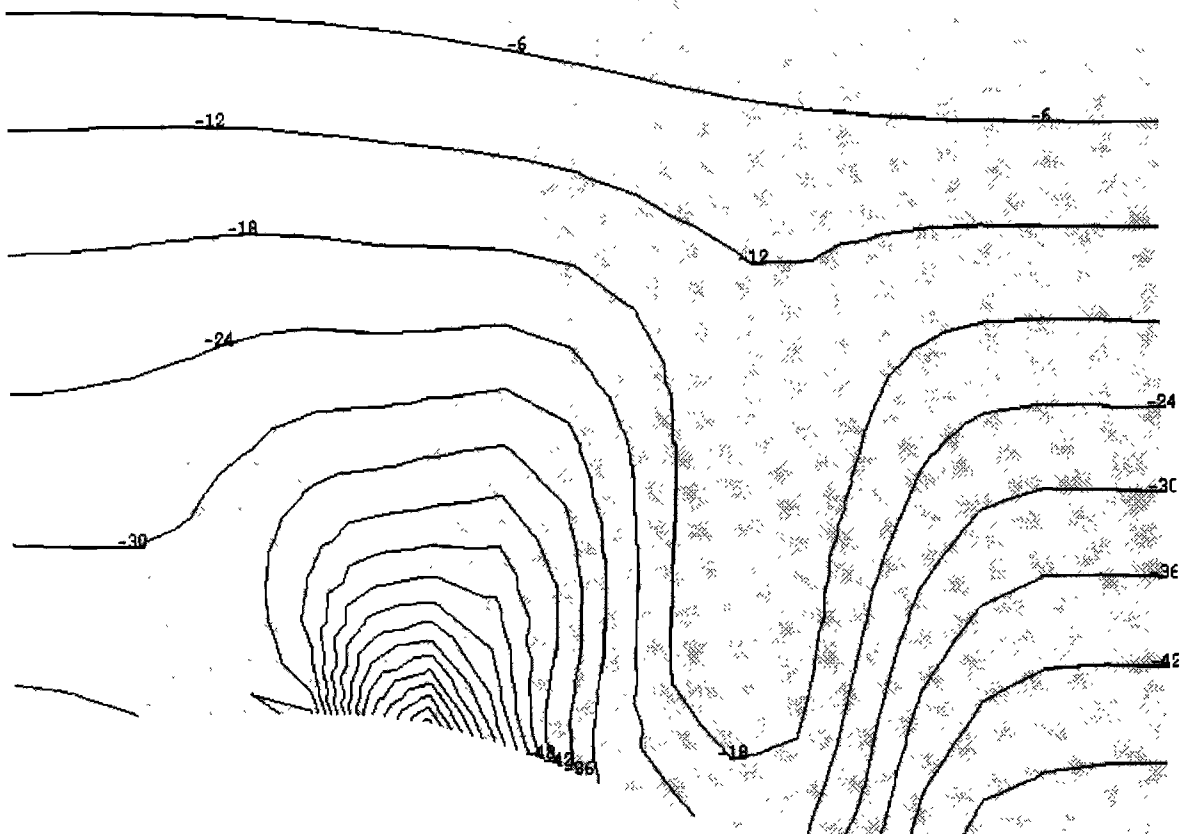
$$\phi_x = \phi_m\left[1 - \sum_{i,\omega} \Delta^{(i\omega)}\right]. \qquad (30)$$

Similarly, the fracture porosity ϕ_f (fraction of the rock volume occupied by fractures) is given by

$$\phi_f = \sum_{i,\omega} \Delta^{(i\omega)}. \qquad (31)$$

Noting that $\phi = \phi_f + \phi_x$, we see that (29) can be used to compute ϕ_x and thus ϕ_m.

The permeability of a fracture described as two parallel, flat walls with mean separation a is equal to $a^2/12$ [*Engelder and*

a

b

Figure 3. Predicted (a) vertical stress and (b) lateral stress distribution in MPa illustrating the effect of shearing on stress.
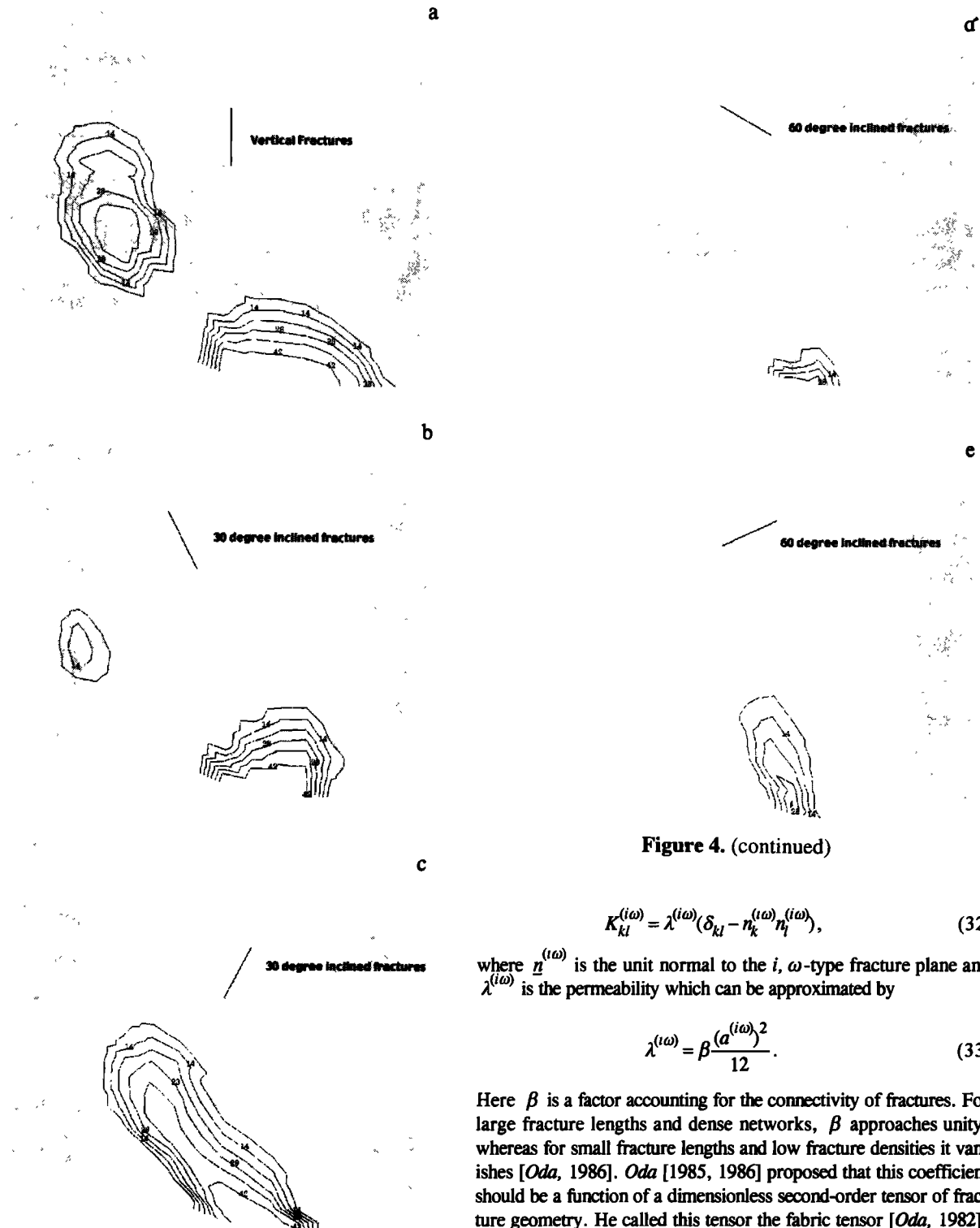
a

Vertical Fractures

b

30 degree inclined fractures

c

30 degree inclined fractures

Figure 4. Predicted contours of fracture length in centimeters for five different orientations.

Scholz, 1981; *Walsh and Brace*, 1984; *Brown*, 1989]. The permeability of a volume element containing a network of parallel fractures may be estimated by multiplying the permeability of a single fracture by the fracture porosity [*Freeze and Cherry*, 1979; *Chen et al.*, 1999]. The anisotropic fracture permeability of a medium consisting of a single fracture type (i, ω) is given by

d

60 degree inclined fractures

e

60 degree inclined fractures

Figure 4. (continued)

$$K_{kl}^{(i\omega)} = \lambda^{(i\omega)}(\delta_{kl} - n_k^{(i\omega)}n_l^{(i\omega)}), \tag{32}$$

where $\underline{n}^{(i\omega)}$ is the unit normal to the i, ω-type fracture plane and $\lambda^{(i\omega)}$ is the permeability which can be approximated by

$$\lambda^{(i\omega)} = \beta \frac{(a^{(i\omega)})^2}{12}. \tag{33}$$

Here β is a factor accounting for the connectivity of fractures. For large fracture lengths and dense networks, β approaches unity, whereas for small fracture lengths and low fracture densities it vanishes [*Oda*, 1986]. *Oda* [1985, 1986] proposed that this coefficient should be a function of a dimensionless second-order tensor of fracture geometry. He called this tensor the fabric tensor [*Oda*, 1982]. A discussion of this factor can be found in the papers of *Oda* [1985, 1986]. In this study β is taken as unity. We assume that the total fracture permeability is obtained by summation of fracture permeabilities for all orientations and statistical classes multiplied by the fracture porosity:

$$\underline{\underline{K}}^{fr} = \sum_{\omega=1}^{N_o} \sum_{i=1}^{N_f} \phi_f^{(i\omega)} \underline{\underline{K}}^{(i\omega)}. \tag{34}$$

This equation has been proposed previously by *Chen et al.* [1999]. It is assumed that fluid flow is slow and the disturbance at fracture
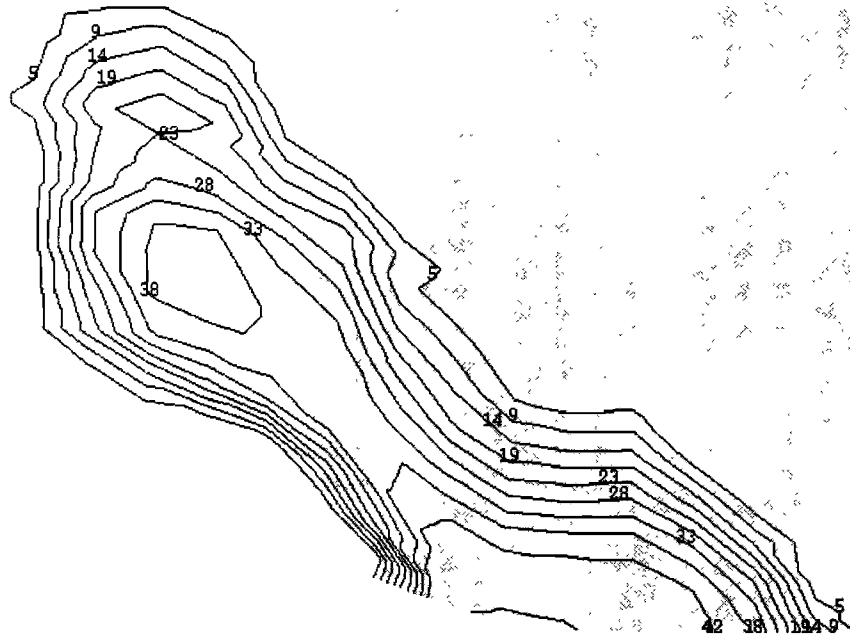
Figure 5. Predicted contours of maximum fracture length in centimeters.

intersections is negligible. Equation (34) is inadequate when the fracture density is lower than the percolation threshold [*Berkowitz*, 1995; *Odling*, 1992; *Bour and Davy*, 1998]. Another limitation is due to the surface roughness of fractures. In this study, fracture aperture is assumed to be constant in a particular fracture. The spatial distribution of fracture aperture alters the fracture permeability. *Waite et al.* [1998] measured water flow through a sinusoidal fracture to compare sinusoidal flow with parallel plate flow. Their experimental and numerical results showed that a sinusoidal fracture has a significantly lower permeability, and for the sinusoidal geometry the effective aperture is very close to the minimum value of the normal aperture. *Thomson and Brown* [1991] showed that the directional nonuniformities in the fracture surface are more important than the degree of surface roughness. Therefore (34) should be viewed as a simple fracture permeability tensor to approximate dense fracture networks with relatively smooth fracture surface. Note that the fracture permeability tensor is obtained by postprocessing the fracture network characteristics. Hence replacement of (34) does not directly affect the fracture model presented in this study.

6. Numerical Approach

In this section, we present the essential equations of the RTM model, numerical approach used, and the nature of the dynamic gridding scheme and the overall flow of the multiprocess coupled

simulation. The strongly coupled nature of the basin deformation problem is captured using an incremental stress rheology (see (1)). The poroelasticity rate of strain $\underline{\dot{\varepsilon}}^{(pe)}$ may be expressed in terms of stress $\underline{\sigma}$, pressure p (of the assumed single) fluid phase, and rock texture Θ via

$$\underline{\dot{\varepsilon}}^{(pe)} = C^{-1}(\Theta)\frac{D}{Dt}(\underline{\sigma} + \alpha(\Theta)p\underline{I}), \tag{35}$$

for fourth-rank matrix of poroelastic coefficients C and effective stress coefficient a; D/Dt represents a material time derivative measuring the rate of change of a tensor in time with respect to a local reference frame fixed to a translating, rotating material point. The texture Θ represents a set of variables characterizing the mineralogy, shape, size, orientation, and packing of the grains. In this study, we assume an isotropic medium represented by two elastic moduli, that is, shear and bulk moduli. These moduli, and the effective stress coefficient of the macroscopic porous medium can be approximately calculated in terms of the grain sizes, composition, porosity, and mineral elastic properties by using *Berryman*'s [1980, 1986] approach.

The inelastic mechanical contribution to $\underline{\dot{\varepsilon}}$ is cast in the present approach as a nonlinear viscosity law in the form

$$\underline{\dot{\varepsilon}}^{(vp)} = \eta^{-1}(\underline{\sigma} + \tilde{\alpha}p\underline{I}). \tag{36}$$

The fourth-rank viscosity tensor η depends on stress, fluid pressure and texture. The second term in the effective stress involves a co-
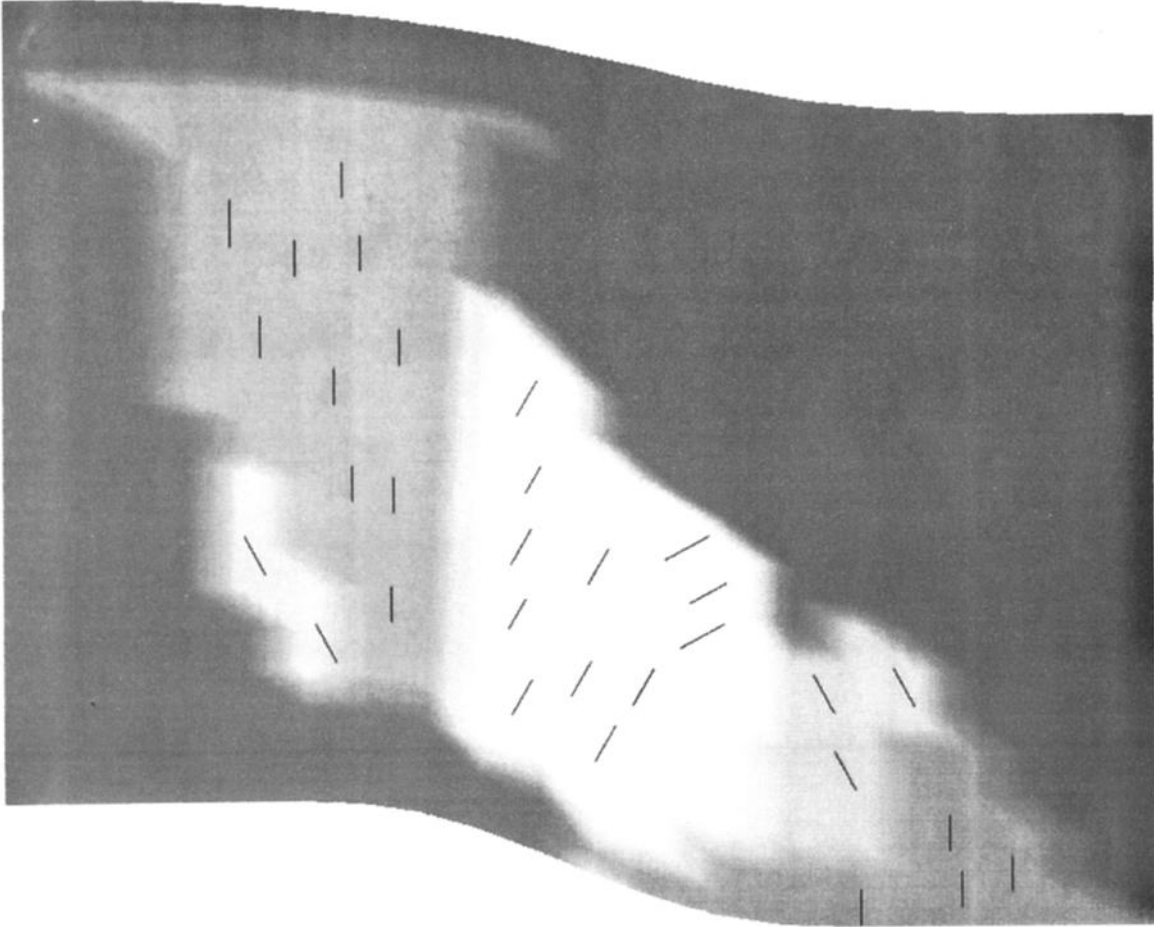
Figure 6. Predicted dominant fracture orientation.

efficient $\tilde{\alpha}$ that is usually taken to be unity. In this study we use the shear and bulk viscosity approximations presented by *Tuncay et al.* [submitted manuscript, 2000].

The force balance equation is

$$\sum_{i'=1}^{3} \frac{\partial \sigma_{ii'}}{\partial x_{i'}} + f_i = 0, \qquad (37)$$

for body force $f_i = g \rho_m \delta_{i3}$. Here g is the gravitational acceleration, ρ_m is the mass density, and the 3-direction is upward.

The fluid mass balance equation can be written as

$$\frac{\partial \phi \rho_f}{\partial t} + \underline{\nabla} \cdot (\phi \underline{v} \rho_f) = 0. \qquad (38)$$

The Darcy law for single fluid phase flow is

$$\phi(\underline{v} - \underline{u}) = -\frac{\underline{\underline{K}}}{\mu_f}\left(\underline{\nabla} p + \rho_f \underline{g}\right). \qquad (39)$$

The substitution of (39) in (38) yields

$$\phi \frac{D\rho_f}{Dt} + \rho_f\left(\frac{D\phi}{Dt} + \phi \underline{\nabla} \cdot \underline{u}\right) = \underline{\nabla} \cdot \frac{\underline{\underline{K}}}{\mu}\left(\underline{\nabla} p + \rho_f \underline{g}\right). \qquad (40)$$

If a state equation in the form of $\rho_f = \rho_f^o(1 + \beta(p - p_o) - \alpha(T - T_o))$ is used, and the mass balance of solids (29) is employed, equation (40) can be rewritten as

$$\phi \beta \rho_f^o \frac{Dp}{Dt} - \phi \alpha \rho_f^o \frac{DT}{Dt} + \rho_f tr(\underline{\dot{\varepsilon}}) = \underline{\nabla} \cdot \frac{\underline{\underline{K}}}{\mu}\left(\underline{\nabla} p + \rho_f \underline{g}\right), \qquad (41)$$

where α and β are the thermal expansivity and compressibility of fluid, respectively, and the superscript o refers to reference values. In this way our fracture network dynamics model is integrated into a coupled multiprocess, crustal deformation/hydrologic model [see also *Ortoleva*, 1998; *Ortoleva et al.*, 1997; *Tuncay et al.*, submitted manuscript, 1999].

In this study, we use the updated Lagrangian approach to analyze the time-dependent large-deformation behavior of geological materials with the incremental stress rheologic behavior [*Bathe et al.*, 1975; *Bathe*, 1996; *Tuncay et al.*, submitted manuscript, 2000]. In our numerical approach, all variables are referred to an updated configuration in each time step. The approach has two major steps. First, the incremental stress rheology is solved at the integration points of the finite elements. Second, the displacements are computed by using a global deformation solver. Iterations of these two steps are performed until the norm of the change in displacements between two consecutive iterations is less than a specified tolerance. The two-step solution technique allows introduction of new deformation mechanisms with only minor changes in the code. We use the conjugate gradient iterative technique with a simple diagonal preconditioner to solve for the incremental displacements. The finite element code and iterative solver are parallelized. We refer to *Tuncay et al.* [submitted manuscript, 2000] for in-depth discussion of the incremental stress rheology and the finite element discretization.

Our simulator is a forward model as suggested in Figure 1. The state of the system at a time t is evolved to a time $t + \delta t$, a short time δt later, by solving the equations of mass, momentum, and energy conservation and textural evolution using three-dimensional
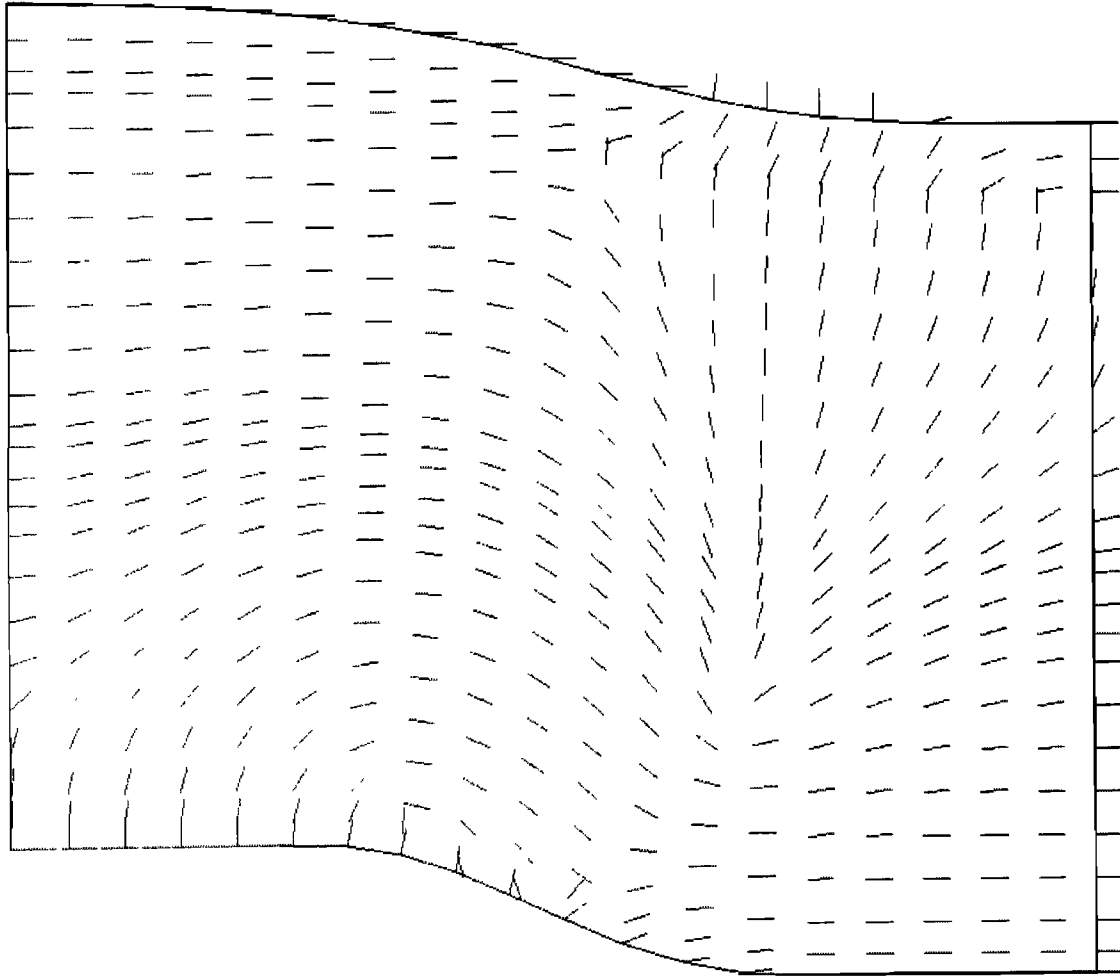
Figure 7. Predicted orientation of the least compressive stress.

finite element methods. All couplings between quantities within the study are preserved by iteration procedures. The present fracture dynamics model is solved in each finite element using the stress, fluid pressure, texture, and temperature there. In turn, the instantaneous state of the fracture network is used to compute the fracture permeability tensor as discussed in the previous sections.

The finite element grid accretes with sediment infilling. A new sediment layer is introduced when the sediment layer at the top of the basin reaches a critical thickness. In contrast, when erosion creates a top layer that is locally too thin, the finite element grid is locally reorganized to preserve numerical accuracy. This accreting, reorganizing grid that also adapts to sedimentary features as they are added (that is, to capture thin beds) is required to capture sedimentary detail and insure numerical stability and accuracy.

7. Numerical Results

To illustrate the multidimensional aspect of fracturing, we applied our model to a two-dimensional normal fault. The system studied consists of alternating sandstone and shale layers (see Figure 2). The initial porosity of sediments is taken as 0.25. Five fracture orientations are considered. Sediment is supplied at a constant rate of 250 m/million years. The right side of the computational domain subsides at a rate of 200m/million years after 3.5 million years into the simulation. After 5 million years, the domain size becomes ap-

proximately 5 km x 1.5 km. The purpose of this simulation is to illustrate the orientation of fractures, anisotropic fracture permeability, and weak zones for such systems. The boundary conditions for the stress/deformation problem are no lateral deformation and no tangential shear stress at the left and right boundaries. Fluid pressure fixes the normal stress at the top, and a specified subsidence profile is imposed at the bottom. For the details of numerical technique, see Tuncay et al. [submitted manuscript, 2000]. Finally, the interplay of the internal reaction, transport, and mechanical processes with the history of overall tectonics, sea level, basement heat flux, and other boundary effects is illustrated in Figure 1.

Figure 2 shows the porosity distribution at 5 million years into the simulation. The four layers are reflected in the porosity variations that emerge even though the porosity was the same at deposition (0.25). Because of the differential subsidence, the porosity in the right third of the domain (darker region at the bottom) is considerably high for two reasons: the relatively low trace of the stress tensor and the contribution of fractures to the porosity there. In our model, porosity is solved from (29). Total porosity is given by the summation of matrix porosity and fracture porosity. Because of the feedback between the fracture mechanics and stress deformation through the volumetric rate of strain due to fracturing, the predicted porosity distribution accounts for both contributions. Differential subsidence results in high compressive stresses on the lower left, yield-
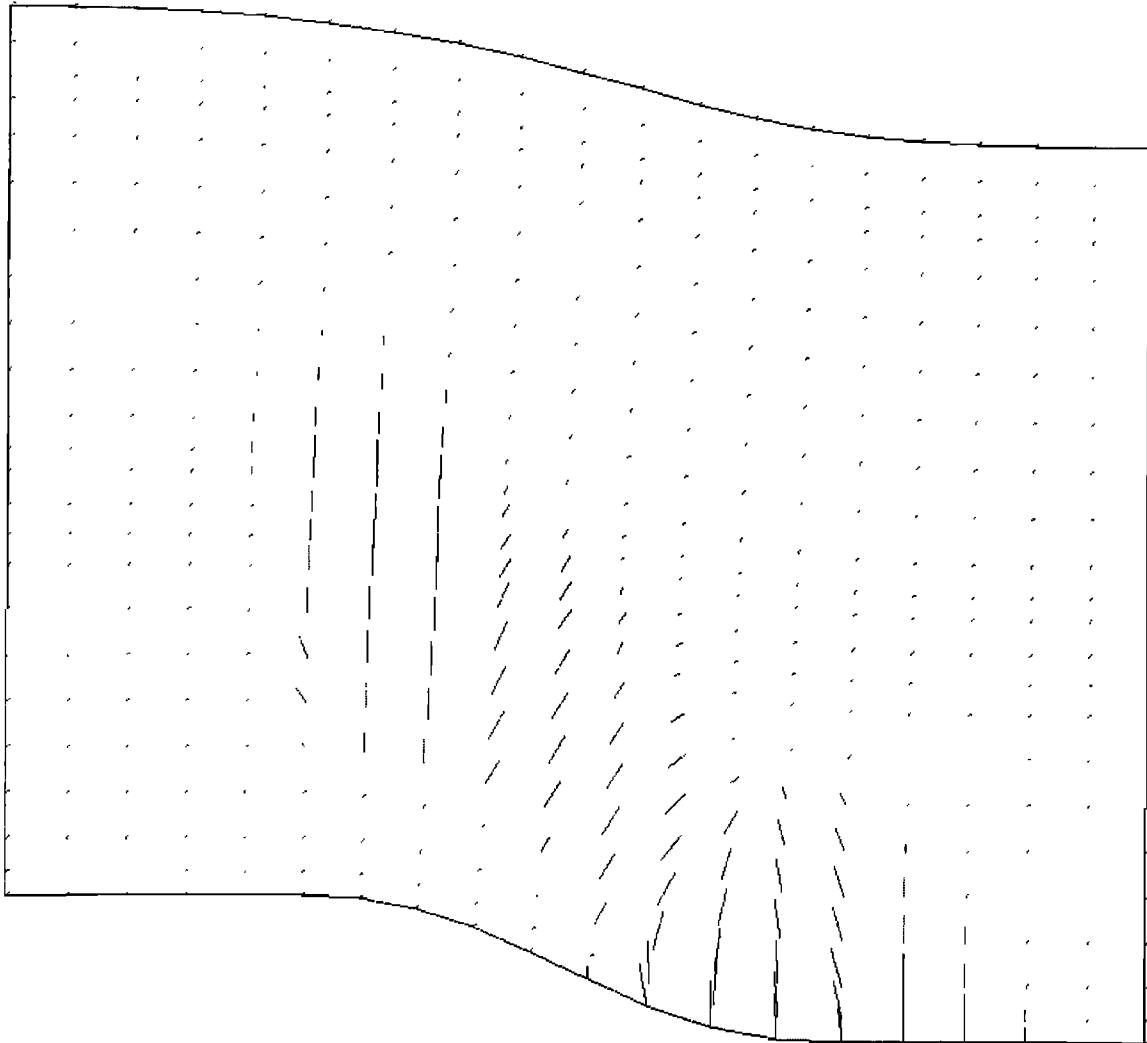
Figure 8. Predicted orientation of the greatest directional fracture permeability scaled with logarithmic fracture permeability.

ing lower porosities (lighter region) there. The light-toned layer in the middle is the first shale layer. Although both shale and sandstone layers start from the same porosity (in this simulation, 0.25), shales compact much faster than sandstones because of their smaller grain size. This figure suggests that the lower zone in the right third of the domain (darker zone at the bottom) and to a lesser extent the region that has relatively high porosity just above and below the shale on the left are likely to fracture.

The contours of vertical stress σ_{zz} and lateral stress σ_{xx} are shown in Figure 3. Note that vertical stress is significantly different than lithostatic stress in the high shear zone. This demonstrates the importance of tensorial aspect of stress for fracturing and faulting. The high porosity zones in Figure 2 are in agreement with low vertical and horizontal stress zones in Figure 3. In most crustal evolution models, it is assumed that rocks fracture when the fluid pressure exceeds a specified fraction of lithostatic stress [*Maubeuge and Lerche*, 1993, 1994; *Roberts and Nunn*, 1995; *Wang and Xie*, 1998]. Clearly, such an approach would fail in this case because of the large spatial variation of stress components induced by the differential subsidence.

In this simulation, five fracture orientations are considered. The contours of fracture length for five different orientations are shown

in Figure 4. Some of the regions overlap, that is, more than one fracture orientation exist (as observed in rock samples). Consider a one-dimensional case, where the least compressive stress is equal to the lateral stress that is independent of orientation. In this particular case, because of the symmetry of the problem, a number of vertical fracture orientations will initiate with equal likelihood. The size and number of fracture orientations mainly depend on fracture propagation velocity and the number of fracture nuclei in a unit volume. Therefore the proposed fracture kinetics model has the power to analyze a variety of problems from one-dimensional identical principal (lateral) stresses to three-dimensional distinct principal stresses. Figure 4c shows that vertical fractures exist in two distinct zones, whereas 60 degree inclined fractures (Figures 4a and 4e) occur in a very limited zone. All five fracture orientations appear in this limited zone. However, fracture lengths of different orientations vary significantly. The largest 60 degree inclined fracture length is 28 cm, whereas 30 degree inclined fractures are as large as 42 cm. Figure 4 demonstrates that even in this simple problem, fractures of different orientation autonomously occur in one or more zones.

Figure 4 can be summarized by plotting the contours of maximum fracture length as shown in Figure 5. In contrast to Figure 4, there is a continuous zone of fractures. However, there are two
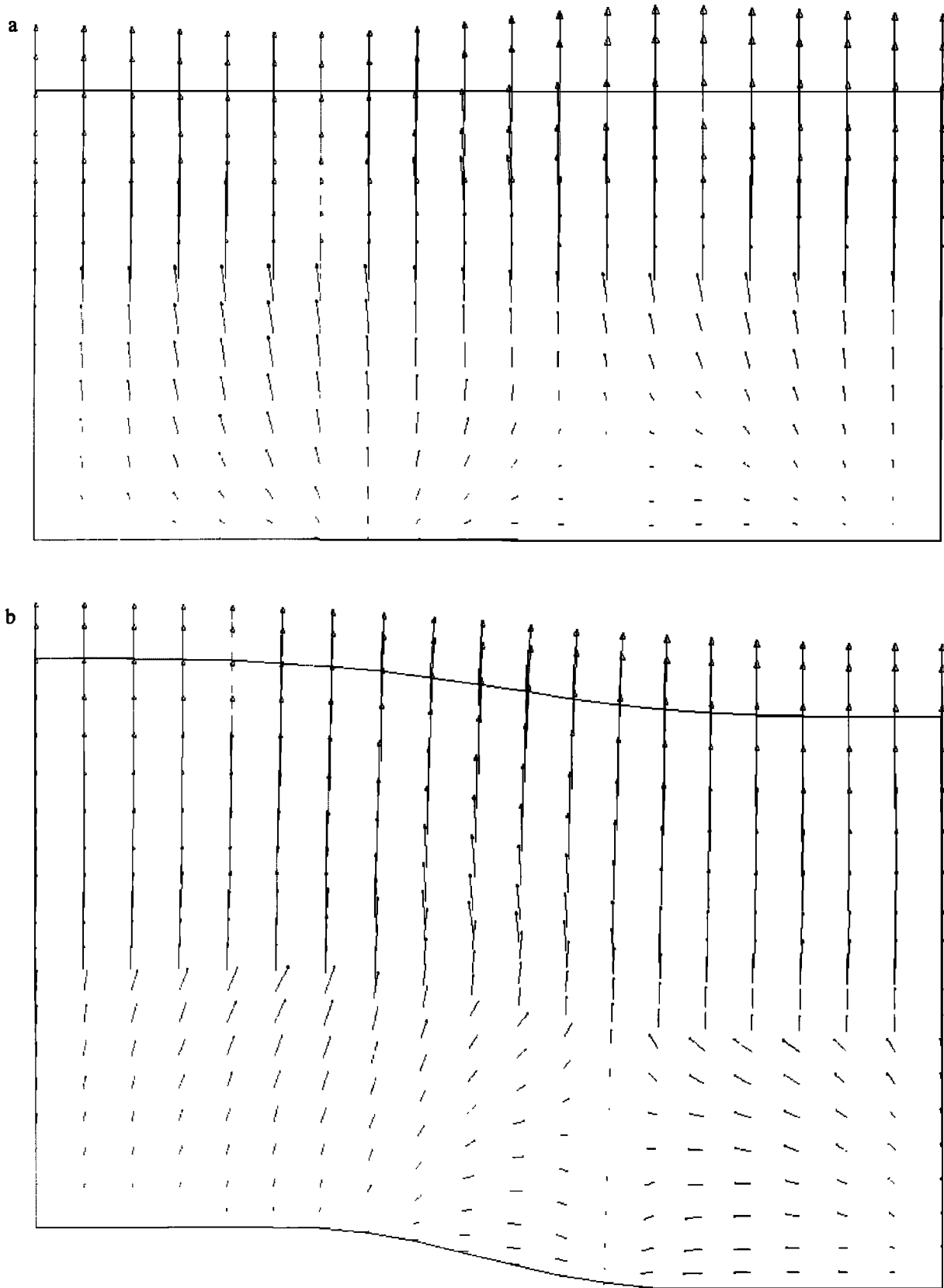
Figure 9. Flow field vectors illustrating the effect of fracturing on fluid flow at (a) 3.51 million years, (b) 3.78 million years, and (c) 5.00 million years.
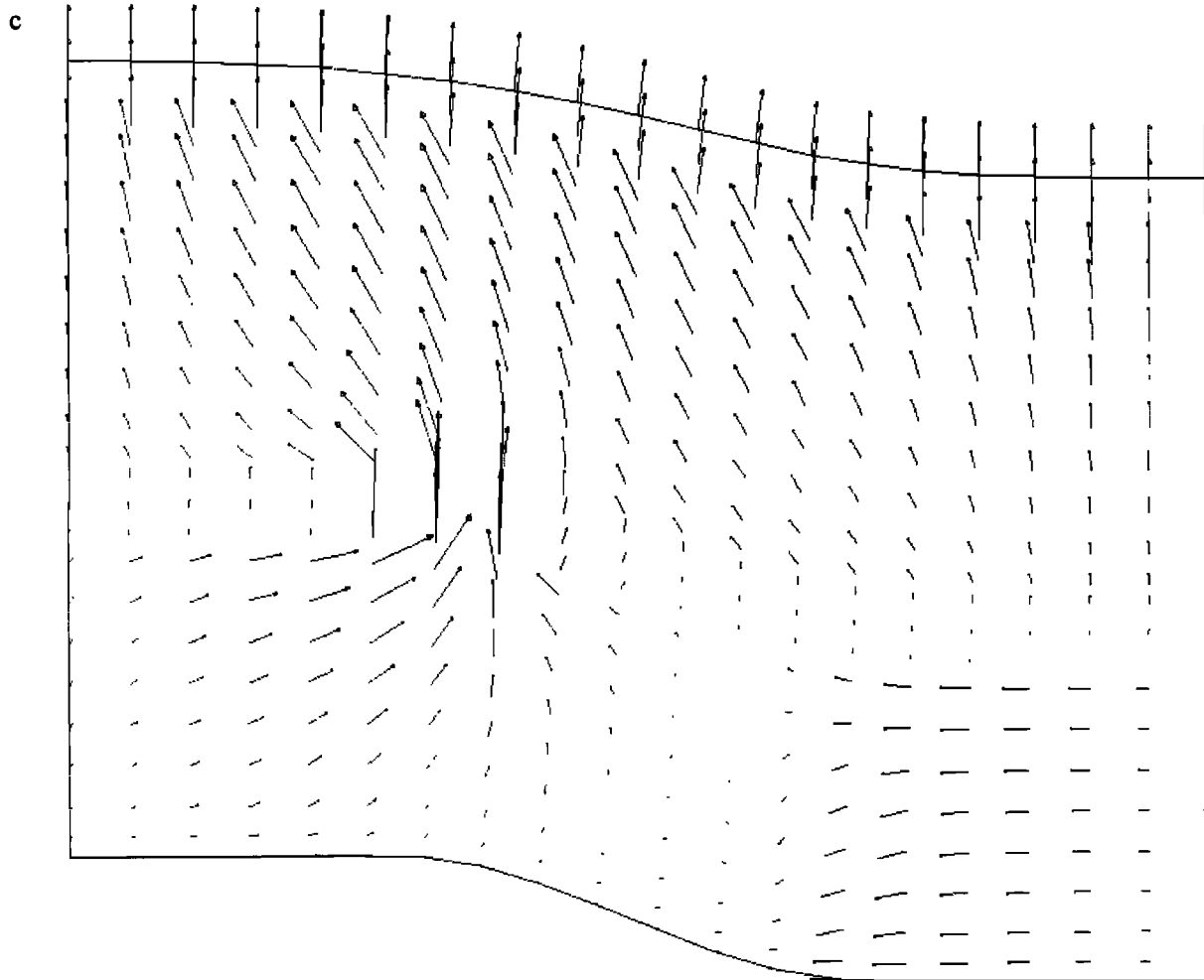
Figure 9. (continued)

zones of large fracture lengths coinciding with vertically fractured zones. It is well known that the initial location and direction of fractures are important factors in the overall evolution of the system. In this particular system, depending on the brittleness of rock and rate of differential subsidence, a number of scenarios is possible. If the system is ductile and rate of differential subsidence is low, fractures are unlikely to occur. If the system is ductile and rate of differential subsidence is high, fractures in a few orientations open because the volumetric strain of fractures that open first will be sufficient to increase the stress component normal to them. Note that in a ductile system, fractures close depending on the elastic and viscous properties of the medium when the differential subsidence stops. If the system is ductile but rate of differential subsidence is very high, fractures in a large number of orientations open. However, the dominant fracture orientation is likely to be the one that opened first. Note that fracture growth rate also significantly affects fracture orientations.

The dominant fracture orientation, that is, orientation with maximum fracture length, is shown in Figure 6. The dark and light shading refer to unfractured and fractured zones, respectively. A simple check of the model can be achieved by comparing the dominant orientation (Figure 6) with least compressive stress orientation (Figure 7) since they must be almost orthogonal.

The complex fracturing pattern results in anisotropic fracture permeability as discussed in the previous sections. Figure 8 shows

the orientation of the greatest directional fracture permeability scaled with logarithmic fracture permeability. This variable can be considered as average fracture orientation scaled with logarithmic fracture permeability. A comparison of Figures 7 and 8 shows that the orientation of the greatest directional fracture permeability is indeed almost orthogonal to the least compressive stress orientation. However, if a complicated time-dependent subsidence pattern was imposed at the bottom, the orthogonality condition might not occur. If the least compressive stress orientation changes at a fast rate, there might be a time delay in the response of the fracture network.

Figure 9 shows the evolution of the fluid flow field. The flow field is one-dimensional until the faulting starts because of the horizontal nature of sediments and boundary conditions. As the differential subsidence starts at 3.5 million years, fractures open and the flow field is strongly affected by both the disturbed symmetry and fractures. As the subsidence continues, two observations are made: the fractured shale layer provides a pathway for fluid escape on the left side, and increasing porosity (due to fracturing) attracts fluids on the lower right side. Note also the shale developed into a seal; however, a fracture-mediated puncture causes local fluid release. Figure 10 combines Figures 2, 5, and 9c to illustrate the relationship between lithology, fracturing, and fluid flow. These results show that even for a relatively simple system as studied here, the spatial distribution of fracture length and aperture can be quite complex.

0.14   0.17   0.20   0.23   0.26
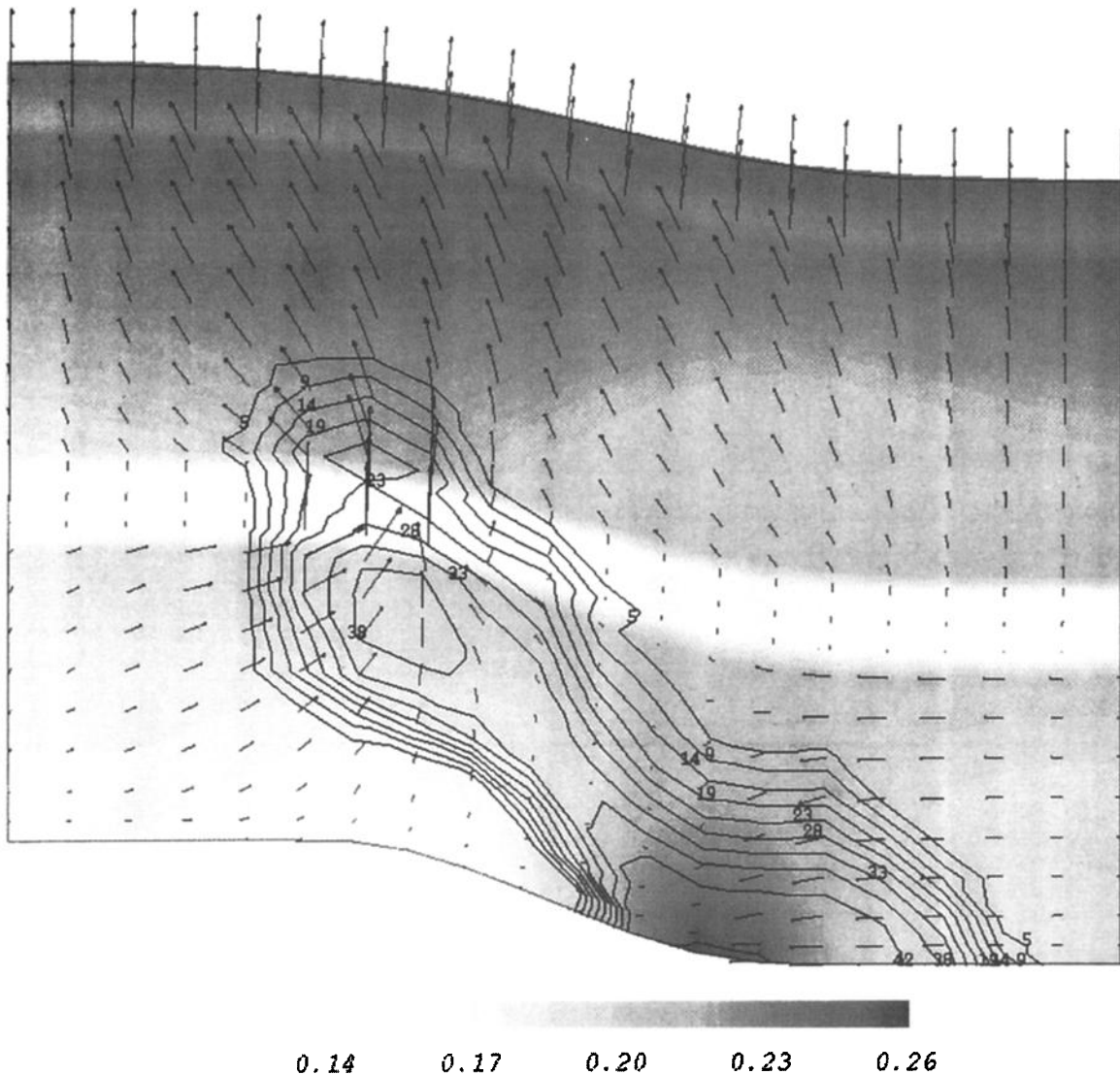
Figure 10. The relationship among variables is captured by our multiprocess fracture model. Shown are the predicted porosity, fracture length, and flow field. The gray-scale background represents porosity and shows differences between four lithologies; lower porosity shales are at the middle and at the top of the domain. Contour lines show the fracture length (centimeters). The arrows indicate the flow field.

8. Conclusions

A new fracture network dynamics model is presented for predicting the statistics of fracture density, length, aperture, and orientation. The influence of fractures on tensorial aspects of fluid flow and rock rheology are delineated. The model allows a putative of orientations which results in complex fracture networks. Our preliminary analysis shows that prediction of fracture networks based on curvature analysis is not reliable since such a correlation does not exist in principle [*Tuncay et al.*, submitted manuscript, 2000]. The same curvature may result in an extensional regime opening fractures in one layer, and in a compressional regime in another. Furthermore, the timing of the curvature development (e.g., folding of a sedimentary rock early in its history when it was poorly lithified) will not lead to fracturing and, even if fractures are induced, they will tend to close in more ductile rocks or become infilled with diagenetic cement. Thus fracture prediction requires a dynamic, forward model.

As mentioned earlier, the approximation used for fracture permeability is based on the assumption of dense networks with smooth fracture surface. It will be interesting to study the effects of a broad distribution of fracture length and aperture, although permeability of such systems does not appear to be developed at this time. Therefore (34) should be viewed as a simple fracture permeability tensor to approximate dense fracture networks with relatively smooth fracture surface. Note that the fracture permeability tensor is obtained by postprocessing the fracture network characteristics. Hence replacement of (34) does not directly affect the fracture model presented in this study.

The coupled fracture mechanics hydrologic system is seen to be able to generate complex spatial patterns of fracturing. In particular, Figure 10 shows two autonomously generated pockets of fracturing existing to the left and right of center. Clearly, in three dimensions, fault dynamics would lead to complex mosaic of fracture-related compartments.

The integrated modeling approach presented here will have predictive power as the reaction, transport, and mechanical laws for a variety of sedimentary rocks improve. An accurate description of time-dependent boundary conditions (such as sedimentation rate, subsidence rate, etc.) is also of great importance for predicting fracture network location and characteristics. As such, our forward modeling approach has great potential value in predictive petroleum exploration and production and fault/earthquake analysis, and more generally, for the dynamics of the crust.

References

Atkinson, B.K., Subcritical crack growth in geological materials, *J. Geophys. Res.*, 89, 4077-4114, 1984.

Bathe, K.J., *Finite Element Procedures*, Prentice Hall, Englewood Cliffs, N. J., 1996.

Bathe, K.J., E. Ramm, and E.L. Wilson, Finite element formulations for large deformation dynamic analysis, *Int. J. Numer. Methods Eng.*, 9, 353-386, 1975.

Berkowitz, B., Analysis of fracture network connectivity using percolation theory, *Math. Geol.*, 27, 467-483, 1995.

Berryman, J.G., Long-wavelength propagation in composite elastic media, I, Spherical inclusions, *J. Acoust. Soc. Am.*, 68, 1809-1819, 1980.

Berryman, J.G., Effective medium approximation for elastic constants of porous solids with microscopic heterogeneity, *J. Appl. Phys.*, 59, 1136-1140, 1986.

Bour, O., and P. Davy, On the connectivity of three-dimensional fault networks, *Water Resour. Res.*, 34, 2611-2622, 1998.

Brantley, S., B. Evans, S.H. Hickman, and D.A. Crerar, Healing of microcracks in quartz: Implications for fluid flow, *Geology*, 18, 136-139, 1990.

Brown, S.R., Transport of fluid and electrical current through a single fracture, *J. Geophys. Res.*, 94, 9429-9438, 1989.

Chen, M., M. Bai, and J.-C. Roegiers, Permeability tensors of anisotropic fracture networks, *Math. Geol.*, 31, 355-373, 1999.

Chen, Y., W. Chen, A. Park, and P. Ortoleva, Role of pressure-sensitive reactions in seal formation and healing: Application of the CIRF.A reaction-transport code, in *Basin Compartments and Seals*, *AAPG Mem.* 61, 403-416, 1994.

Currie, J.B., and S.O. Nwachukwu, Evidence on incipient fracture porosity in reservoir rocks at depth, *Bull. Can. Pet. Geol.*, 22, 42-58, 1974.

Dewers, T., and P. Ortoleva, Non-linear dynamics in chemically compacting porous media, in *Modeling and Analysis of Diffusive and Advective Processes in Geosciences*, edited by W.E. Fitzgibbon and M.F. Wheeler, pp. 100-121, Soc. of Ind. and Appl. Math., Philadelphia, Pa., 1992.

Dewers, T., and P. Ortoleva, Nonlinear dynamical aspects of deep basin hydrology: Fluid compartment formation and episodic fluid release, *Am. J. Sci.*, 294, 713-755, 1994.

Domenico, P.A., and V.V. Palciauskas, The generation and dissipation of abnormal fluid pressures in active depositional environments, in *Hydrogeology*, vol. 1, edited by W. Back, J.S. Rosenshein, and P.R. Seaber, pp. 435-445, Geol. Soc. of Am., Boulder, Co., 1988.

Dutton, R., The propagation of cracks by diffusion, in *Fracture Mechanics of Ceramics*, vol. 2, *Symposium on the Fracture Mechanics of Ceramics*, edited by R.C. Bradt, D.P.H. Hasselman, and F.F. Lange, pp. 649-657, Plenum, New York, 1974.

Engelder, T, Joints and shear fractures in rock, in *Fracture Mechanics of Rocks*, edited by B.K. Atkinson, pp. 27-69, Academic, San Diego, Calif., 1987.

Engelder, T., and P. Geiser, On the use of regional joint sets as trajectories of paleostress fields during the development of the Appalachian Plateau, New York, *J. Geophys. Res.*, 85, 6319-6341, 1980.

Engelder, T., and C.H. Scholz, Fluid flow along very smooth joints at

effective pressures up to 200 megapascals, in *Mechanical Behavior of Crustal Rocks, Geophys. Monogr. Ser.*, vol. 24, edited by N.L. Carter et al., pp. 147-152, AGU, Washington, D. C., 1981.

Etheridge, M.A., V.J. Wall, and R.H. Vernon, The role of fluid phase during regional metamorphism and deformation, *J. Metamorph. Geol.*, 1, 205-226, 1983.

Fischer, M.P., M.R. Gross, T. Engelder, and R.J. Greenfield, Finite element analysis of the stress distribution around a pressurized crack in layered elastic medium: Implications for the spacing of fluid-driven joints in bedded sedimentary-rock, *Tectonophysics*, 247, 49-64, 1995.

Freeze, R.A, and J.A. Cherry, *Groundwater*, Prentice-Hall, Englewood Cliffs, N. J., 1979.

Friedman, M., Fracture in rock, *Rev. Geophys.*, 13, 352-358, 1975.

Ghaith, A., W. Chen, and P. Ortoleva, Oscillatory methane release from shale source rock, *Earth Sci. Rev.*, 29, 241-248, 1990.

Gross, M.R., The origin and spacing of cross joints: Examples from the Monterey formation, Santa-Barbara coastline, California, *J. Struct. Geol.*, 15, 737-751, 1993.

Hancock, P.L., A. Al Kadhi, and J.L. Walper, Regional joint sets in the Arabian platform as indicators of intraplate processes, *Tectonophyiscs*, 3, 27-43, 1984.

Harris, J.F., G.L. Taylor, and J.L. Walper, Relation of deformational fractures in sedimentary rocks to regional and local structures, *AAPG Bull.*, 44, 1853-1873, 1960.

Koudina, N., R.G. Garcia, J.-F. Thovert, and P.M. Adler, Permeability of three-dimensional fracture networks, *Phys. Rev. E*, 57, 4466-4479, 1998.

Kulander, B.R., C.C. Barton, and S.L. Dean, The application of fractography to core and outcrop fracture investigations, *Rep. METC/SP-79/3*, 174 pp., U.S. Dep. of Energy, Morgantown Energy Tech. Cent., Morgantown, WV, 1979.

Long, J.C.S., and D.M. Billaux, From field theory to fracture network modeling: An example incorporating spatial structure, *Water Resour. Res.*, 23, 1201-1216, 1987.

Lorenz, J.C., L.W. Teufel, and N.R. Warpinski, Regional fractures, I, A mechanism for the formation of regional fractures at depth in flat-lying reservoirs, *AAPG Bull.*, 75, 1714-1737, 1991.

Luo, X., and G. Vasseur, Geopressuring mechanism of organic matter cracking: Numerical modeling, *AAPG Bull.*, 80, 856-873, 1996.

Mallory, W.W., Oil and gas from fractured shale reservoirs in Colorado and northwest New Mexico, Rocky Mt. Assoc. of Geol. *Spec. Pub. 1*, 38 pp., Denver, Colo., 1977.

Maubeuge, F., and I. Lerche, A north Indonesian basin: Geo, thermal and hydrocarbon generation histories, *Mar. Pet. Geol.*, 10, 231-245, 1993.

Maubeuge, F., and I. Lerche, Geopressure evolution and hydrocarbon generation in a north Indonesian basin: Two-dimensional quantitative modelling, *Mar. Pet. Geol.*, 104, 104-115, 1994.

Maxwell, J.M., The physical chemistry and nonlinear dynamics of compartment formation in sedimentary basins, Ph.D. dissertation, Indiana Univ., Bloomington, 1997.

Nickelsen, R.P., and V.N.D. Hough, Jointing in the Appalachian Plateau of Pennsylvania, *Geol. Soc. Am. Bull.*, 78, 609-630, 1967.

Oda, M., Fabric tensor for discontinous geological materials, *Soils Found.*, 22, 96-108, 1982.

Oda, M., Permeability tensor for discontinous rock masses, *Geotechnique*, 35, 483-495, 1985.

Oda, M., An equivalent continuum model for coupled stress and fluid flow analysis in jointed rock masses, *Water Resour. Res.*, 22, 1845-1856, 1986.

Odling, N.E., Network properties of a two-dimensional natural fracture pattern, *Pure Appl. Geophys.*, 138, 95-114, 1992.

Ortoleva, P., *Geochemical Self-Organization*, Oxford Univ. Press, New York, 1994a.

Ortoleva, P. (Ed.), *Basin Compartments and Seals, AAPG Mem. 61*, 477 pp., 1994b.

Ortoleva, P., Basin Compartments and Seals, *Rep. GRI-97/0097*, 289 pp., Gas Res. Inst., Chicago, IL, 1998.

Ortoleva, P., J.M. Maxwell, D. Payne, W. Sibo, and J. Comer, Naturally fractured reservoirs and compartments: A predictive basin modeling approach, in *Fractured Reservoirs: Characterization and Modeling*, edited by T.E. Hoak, A.L. Klawitter, and P.K. Blomquist, pp. 67-102, Rocky Mt. Assoc. of Geol., Denver, Colo., 1997.

Ortoleva, P., E. Merino, J. Chadam, and C.H. Moore, Geochemical

self-organization, I, Reaction-transport feedback mechanisms and modeling approach, *Am. J. Sci., 287*, 979-1007, 1987a.

Ortoleva, P., E. Merino, C.H. Moore, and J. Chadam, Geochemical self-organization, II, The reactive-infiltration instability, *Am. J. Sci., 287*, 1008-1040, 1987b.

Pollard, D.D., and A. Aydin, Progress in understanding jointing over the past century, *Geol. Soc. Am. Bull., 100*, 1181-1204, 1988.

Rice, J.R., and J.W. Rudnicki, Earthquake precursor effects due to pore fluid stabilization of a weakening fault zone, *J. Geol. Res., 84*, 2177-2193, 1979.

Roberts, S.J., and J.A. Nunn, Episodic fluid expulsion from geopressured sediments, *Mar. Pet. Geol., 12*, 195-204, 1995.

Schneider, F., J.L. Potdevin, S. Wolf, and I. Faille, Mechanical and chemical compaction model for sedimentary basin simulators, *Tectonophysics, 263*, 307-317, 1996.

Segall, P., Rate-dependent extensional deformation resulting from crack growth in rock, *J. Geophys. Res., 89*, 4185-4195, 1984.

Segall, P. and D.D. Pollard, Joint formation in granitic rock of the Sierra Nevada, *Geol. Soc. Am. Bull., 94*, 563-575, 1983.

Sleep, N.H., Trapping of melt by veins and dikes, *J. Geophys. Res., 93*, 10255-10272, 1988.

Smith, D.L., and B. Evans, Diffusional crack healing in quartz, *J. Geophys. Res., 89*, 4125-4135, 1984.

Sonnenthal, E., and P. Ortoleva, Numerical simulations of overpressured compartments in sedimentary basins, in *Basin Compartments and Seals, AAPG Mem. 61*, 403-416, 1994.

Swanson, P.L., Subcritical crack growth and other time- and environmental-dependent behavior in crustal rocks, *J. Geophys. Res., 89*, 4137-4152, 1984.

Thomson, M.E., and S.R. Brown, The effect of anisotropic surface roughness on flow and transport in fractures, *J. Geophys. Res., 96*, 21923-21932, 1991.

Ungerer, P., J. Burrus, B. Doligez, P.Y. Chenet, and F. Bessis, Basin evaluation by integrated two-dimensional modeling of heat transfer, fluid flow, hydrocarbon generation, and migration, *AAPG Bull., 74*, 309-335, 1990.

Waite, M.E., S. Ge, H. Spetzler, and D.B. Bahr, The effect of surface geometry on fracture permeability: A case study using a sinusoidal fracture, *Geophys. Res. Lett., 25*, 813-816, 1988.

Walsh, J.B., and W.F. Brace, The effect of pressure on porosity and the transport properties of rocks, *J. Geophys. Res., 89*, 9425-9431, 1984.

Wang, C., and X. Xie, Hydrofracturing and episodic fluid flow in shale-rich basins: A numerical study, *AAPG Bull., 82*, 1857-1869, 1998.

Wang, J.S.Y., C.F. Tang, and R.A. Sternbentz, The state of the art of numerical modeling of thermohydrologic flow in fractured rock masses, *Environ. Geol., 4*, 133-199, 1983.

Wu, H.Q., and D.D. Pollard, An experimental study of the relationship between joint spacing and layer thickness, *J. Struct. Geol., 17*, 887-905, 1995.

P. Ortoleva, A. Park, and K. Tuncay, Laboratory for Computational Geodynamics, Department of Chemistry, Chemistry Building, Indiana University, Bloomington, IN 47405. (ortoleva@indiana.edu; park2@indiana.edu; ktuncay@indiana.edu)